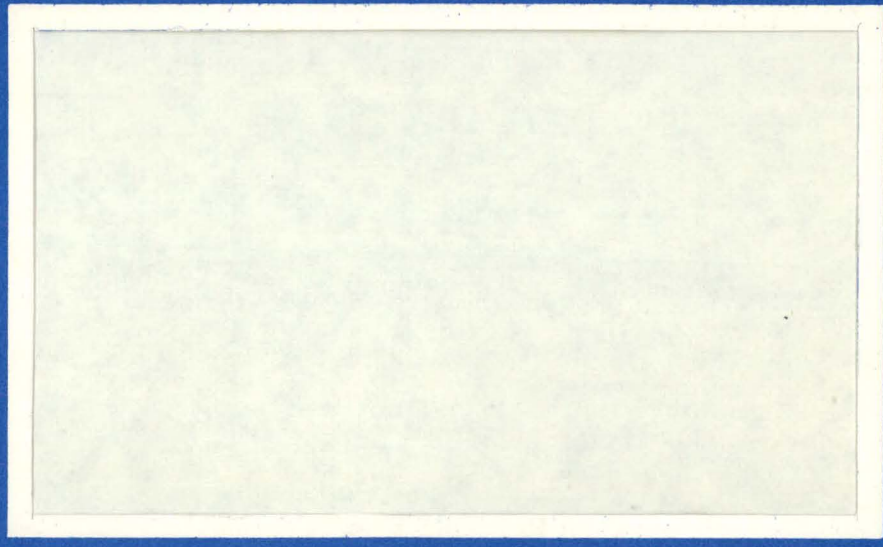


227  
1-11-71

DR-1624



MASTER



**WADCO**  
CORPORATION

a subsidiary of Westinghouse Electric Corporation  
Post Office Box 1970  
Richland, Washington 99352



DISTRIBUTION OF THIS DOCUMENT IS UNLIMITED

180

## DISCLAIMER

**This report was prepared as an account of work sponsored by an agency of the United States Government. Neither the United States Government nor any agency Thereof, nor any of their employees, makes any warranty, express or implied, or assumes any legal liability or responsibility for the accuracy, completeness, or usefulness of any information, apparatus, product, or process disclosed, or represents that its use would not infringe privately owned rights. Reference herein to any specific commercial product, process, or service by trade name, trademark, manufacturer, or otherwise does not necessarily constitute or imply its endorsement, recommendation, or favoring by the United States Government or any agency thereof. The views and opinions of authors expressed herein do not necessarily state or reflect those of the United States Government or any agency thereof.**

## **DISCLAIMER**

**Portions of this document may be illegible in electronic image products. Images are produced from the best available original document.**



**NOTICE**

This report was prepared as an account of work sponsored by the United States Government. Neither the United States nor the United States Atomic Energy Commission, nor any of their employees, nor any of their contractors, subcontractors, or their employees, makes any warranty, express or implied, or assumes any legal liability or responsibility for the accuracy, completeness or usefulness of any information, apparatus, product or process disclosed, or represents that its use would not infringe privately owned rights.

**HANFORD ENGINEERING DEVELOPMENT LABORATORY**

Richland, Washington  
operated by

**WADCO CORPORATION**

A Subsidiary of Westinghouse Electric Corporation  
for the

United States Atomic Energy Commission Under Contract No. AT(45-1)-2170

COMPARISON OF NUCLEAR DESIGN MODELS  
FOR POWER AND FLUX DISTRIBUTIONS  
NEAR THE FTR CORE-REFLECTOR INTERFACE

L. D. O'Dell  
R. B. Rothrock

November 1970

FIRST UNRESTRICTED  
DISTRIBUTION MADE

DEC 29 '70

LEGAL NOTICE

This report was prepared as an account of work sponsored by the United States Government. Neither the United States nor the United States Atomic Energy Commission, nor any of their employees, nor any of their contractors, subcontractors, or their employees, makes any warranty, express or implied, or assumes any legal liability or responsibility for the accuracy, completeness or usefulness of any information, apparatus, product or process disclosed, or represents that its use would not infringe privately owned rights.



**WADCO**  
CORPORATION  
Richland, Washington 99352

UNCLASSIFIED

DISTRIBUTION OF THIS DOCUMENT IS UNLIMITED

Printed in the United States of America  
Available from  
National Technical Information Service  
National Bureau of Standards,  
U.S. Department of Commerce  
Springfield, Virginia 22151  
Price: Printed Copy \$3.00; Microfiche \$0.65

COMPARISON OF NUCLEAR DESIGN MODELS  
FOR POWER AND FLUX DISTRIBUTIONS  
NEAR THE FTR CORE-REFLECTOR INTERFACE

L. D. O'Dell  
R. B. Rothrock

ABSTRACT

Diffusion and transport ( $S_n$ ) calculations in one and two dimensions are described. The objective of this study is to determine the model detail required to accurately calculate flux and power distributions near the Fast Test Reactor (FTR) core-reflector interface.

**THIS PAGE  
WAS INTENTIONALLY  
LEFT BLANK**



CONTENTS

LIST OF FIGURES	vii
LIST OF TABLES	vii
1.0 INTRODUCTION	1
2.0 ONE-DIMENSIONAL SPHERICAL CALCULATIONS	2
2.1 Cases Compared	2
2.2 Effects of Scattering Anisotropy in Sn Calculations	3
2.3 Effects of Angular Detail in Flux Description	5
2.4 Effects of Energy Resolution	5
2.5 Effects of Cross-Section Resonance Shielding	7
2.6 Effect of Spatial Resolution	9
3.0 TWO-DIMENSIONAL CALCULATIONS	9
3.1 XY Calculations	9
3.2 Results of Triangular Geometry Calculations	14
4.0 CONCLUSIONS	17
REFERENCES	19
APPENDIX A	20

LIST OF FIGURES

2.1	Effects of Scattering Anisotropy in Sn Calculations Near Core-Reflector Interface	4
2.2	Effect of Angular Detail and Energy Resolution near Core-Reflector Interface	6
2.3	Comparison of Flux Spectra at Core Center and Core-Reflector Boundary, from Case 1 (S8-P3)	8
3.1	Geometry for XY Calculations	10
3.2	Total Flux Traverse Through B <sub>4</sub> C Rod	11
3.3	Total Flux Traverse Just Outside B <sub>4</sub> C Rod	12
3.4	Blowup of Flux Traverse Through B <sub>4</sub> C Rod	12
3.5	Blowup of Flux Traverse Just Outside B <sub>4</sub> C Rod	13
3.6	Half-Core Hexagonal Geometry	14
3.7	Total Flux and Power Density Traverse "A"	16
3.8	Total Flux and Power Density Traverse "B"	16

LIST OF TABLES

2.1	One-Dimensional Cases Compared	2
3.1	Two-Dimensional XY Calculations	11
3.2	Averaged Group Fluxes Obtained from 6 and 24 Mesh Triangle Per Hexagonal Calculations	17

COMPARISON OF NUCLEAR DESIGN MODELS  
FOR POWER AND FLUX DISTRIBUTIONS  
NEAR THE FTR CORE-REFLECTOR INTERFACE

L. D. O'Dell  
R. B. Rothrock

1.0 INTRODUCTION

Various one-dimensional (1D) and two-dimensional (2D) diffusion and transport ( $S_n$ ) calculations were performed to determine the model detail necessary to accurately calculate flux and power distributions in the Fast Test Reactor (FTR) near the core-reflector boundary. The codes employed in these calculations were the IDX<sup>(1)</sup> and 2DB<sup>(2)</sup> diffusion codes and the ANISN<sup>(3)</sup> and DOT<sup>(4)</sup> transport ( $S_n$ ) codes. The  $S_n$  quadrature parameters used in the transport calculation were obtained from Lee's documentation.<sup>(5)</sup> Compositions and overall dimensions are intended to be representative of the FTR.

Two sets of cross-sections were employed throughout the calculations; the 26-group FTR-III cross-section set<sup>(6)</sup> (a modified version of the Bondarenko cross-sections) and a 27-group set reduced from a 100 group GAM-II set (3/22/67-Tape #408). This 27-group set contained anisotropic scattering moments through P3 but were not resonance shielded.

Nuclear behavior at the fuel/reflector interface was examined with a series of one-dimensional calculations, described in Section 2. Two-dimensional effects near peripheral poison rod locations were studied with a simple quarter core XY model having a single boron carbide poison rod at the core edge, and the effect of mesh size in triangular geometry diffusion calculations was evaluated with a detailed half core model. These latter calculations are described in Section 3. Conclusions reached from results of these calculations are listed in Section 4.

## 2.0 ONE-DIMENSIONAL SPHERICAL CALCULATIONS

### 2.1 CASES COMPARED

One-dimensional flux and fission neutron distributions were calculated for a spherical representation of the FTR containing two fuel zones and a reflector. These calculations were all normalized to a total fission neutron source rate of 1.0 and were performed with IDX<sup>(1)</sup> and ANISN<sup>(3)</sup>. Identical geometry and compositions were used in all cases (see Appendix A). The cases compared are tabulated in Table 2.1 along with the calculated eigenvalues and relative reflector peaks. These reflector peaks are a measure of the power peaking effect of the soft neutron spectrum returning from the reflector. They are calculated as the ratio of the power density in the outermost core mesh interval to the power density at the "trough" of the reflector peak (usually 1 or 2 cm inside the core).

TABLE 2.1  
ONE-DIMENSIONAL CASES COMPARED

Case	Model	Scattering Treatment	Computer Code	Cross-Section Set	Calculated Eigenvalue	Relative Reflector Peak
1	S8	P3	ANISN	27 Group <sup>(a)</sup>	1.1463	7.3%
2	S8	P1	ANISN	27 Group <sup>(a)</sup>	1.1459	7.4
3	S8	P0	ANISN	27 Group <sup>(a)</sup>	1.1791	6.3
4	S2 <sup>(b)</sup>	--	ANISN	27 Group <sup>(a)</sup>	1.1569	9.9
5	S8	TA <sup>(c)</sup>	ANISN	21 Group <sup>(d)</sup>	1.1277	0.7
6	S4	TA	ANISN	21 Group <sup>(d)</sup>	1.1280	0.8
7	S4	TA	ANISN	11 Group <sup>(d)</sup>	1.1270	0.3
8	S4	TA	ANISN	6 Group <sup>(d)</sup>	1.1311	0.3
9	DIFF.	TA	IDX	21 Group <sup>(d)</sup>	1.1239	1.3
10	DIFF.	TA	IDX/PERT V <sup>(7)</sup>	21 Group <sup>(e)</sup>	1.1239	6.0

a. Unshielded.

b. Modified S2 diffusion calculation.

c. Transport approximation.

d. Resonance self-shielded; collapsed from FTR-III 26-group set.

e. Flux distribution calculated with shielded cross-sections; power density near reflector represented by activation traverse using unshielded Pu<sup>239</sup> fission cross section.

## 2.2 EFFECTS OF SCATTERING ANISOTROPY IN $S_n$ CALCULATIONS

The fission neutron source density near the reflector as calculated by ANISN<sup>(3)</sup> in S8-P0, S8-P1, and S8-P3 is shown in Figure 2.1. The P1 and P3 results are indistinguishable on the graph, while the P0 case differs significantly. This difference between the P3 and P0 case is magnified by the large difference in the calculated eigenvalues which is also present in the curves. These comparisons do suggest, however, that retention of linearly anisotropic scattering components is necessary for an accurate description of the power shape near the interface, while higher order scattering moments can be ignored. A direct comparison of SN-P1 and SN-TA (transport approximation) results could not be readily made since the anisotropic cross-section set used does not include a transport cross section, and considerable editing of cross-section tapes would be required to produce directly comparable SN-P1 and SN-TA results.

The general behavior of the transport approximation may be inferred, however, from reported studies in which directly comparable monoenergetic calculations were performed with TA and PL scattering treatments.<sup>(8)</sup> Effects of various scattering representations on detailed flux distributions near discontinuities can be judged from the results presented for the flux near a plane source, in a medium characterized by hydrogen scattering with an average of 0.9 secondaries per collision. Maximum flux deviations near the source of about 5 percent were found between transport approximation and P4 results in this rather strongly anisotropic case. Anisotropic scattering in the FTR core is comparatively much weaker, due to the greater mass of scatterers, up to the energy range where the scattering process becomes asymmetric; this includes the majority of the neutrons causing fissions, and especially those returning from the

reflector. Flux levels are low in the high energy groups where departures from spherically symmetric scattering become appreciable. It is believed that the transport approximation predicts flux and power distributions near discontinuities in the FTR within a few percent, with the possible exception of the highest energy flux groups which do not contribute significantly to the power density.

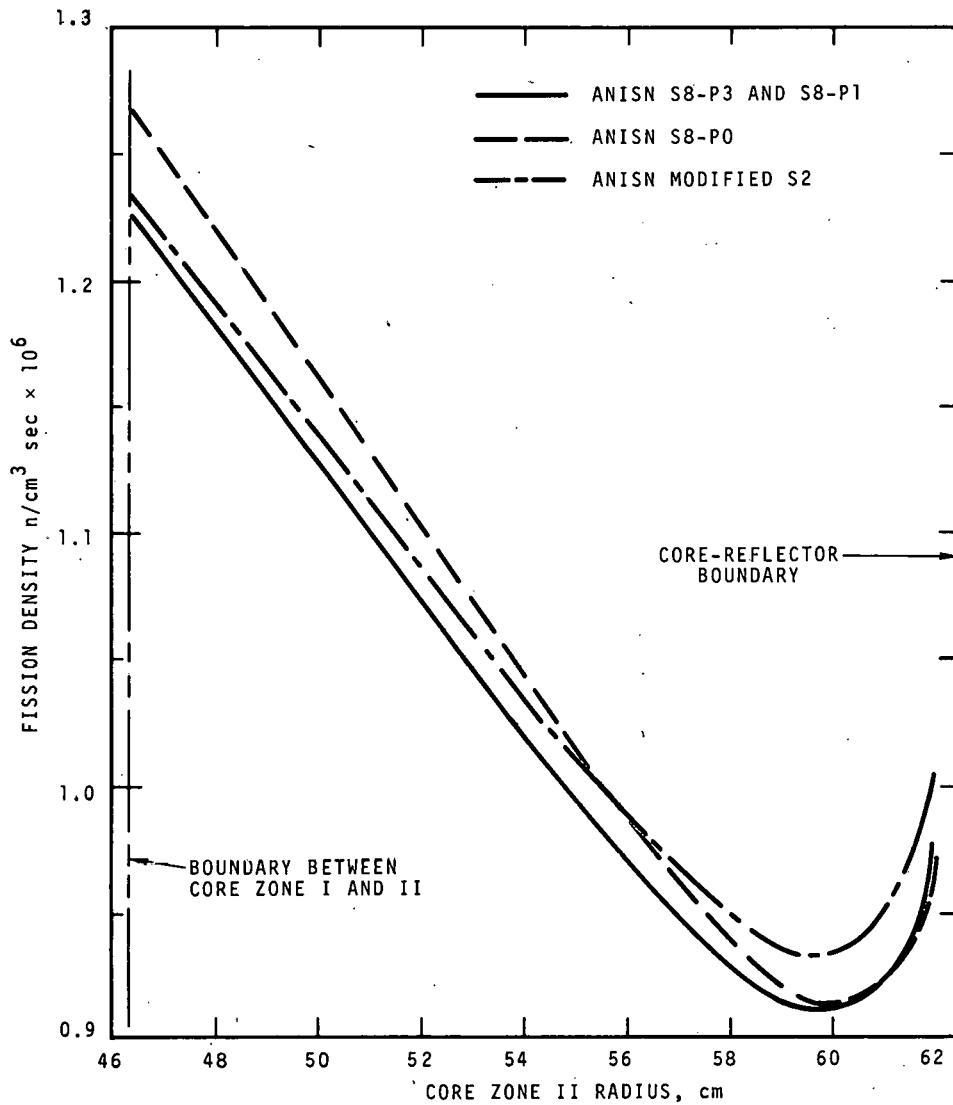


**FIGURE 2.1.** Effects of Scattering Anisotropy in Sn Calculations Near Core-Reflector Interface

### 2.3 EFFECTS OF ANGULAR DETAIL IN FLUX DESCRIPTION

The effects of angular detail on flux and power distributions near the core-reflector interface are shown in Figures 2.1 and 2.2. In Figure 2.1, a comparison is shown between S8 results and a modified S2 calculation using the 27 group unshielded cross-section set. In Figure 2.2, the comparison is between an ANISN<sup>(3)</sup> S8 and S4 calculation and a 1DX<sup>(1)</sup> calculation using a 21-group set generated from the 26-group FTR-III cross-section set.<sup>(6)</sup> An examination of these cases reveals the following trends:

- a) Calculated neutron energy spectra at the core edge are essentially independent of the angular resolution in the flux; in the energy groups where a perceptible difference occurs, the lower-order calculation appears to yield a slightly softer spectrum.
- b) When normalized to the same total fission rates, the lower order calculations show higher flux levels at the core-reflector boundary than do the higher order calculations. The magnitude of the difference varies with cross-section set and the number of energy groups.

Due to these trends in the calculated flux distribution, the lower order approximations (S2 or diffusion theory) consistently predicted higher peaking effects at the core edge than did the S8 calculations (see Table 2.1).

### 2.4 EFFECTS OF ENERGY RESOLUTION

The effects of different energy resolution (cross-section collapsing) can be inferred from a comparison of Cases 6, 7, and 8 (see Table 2.1 and Figure 2.2) which used 21, 11, and 6 energy groups, respectively, in otherwise identical calculations. In these cases, the reflector peak was reduced to less



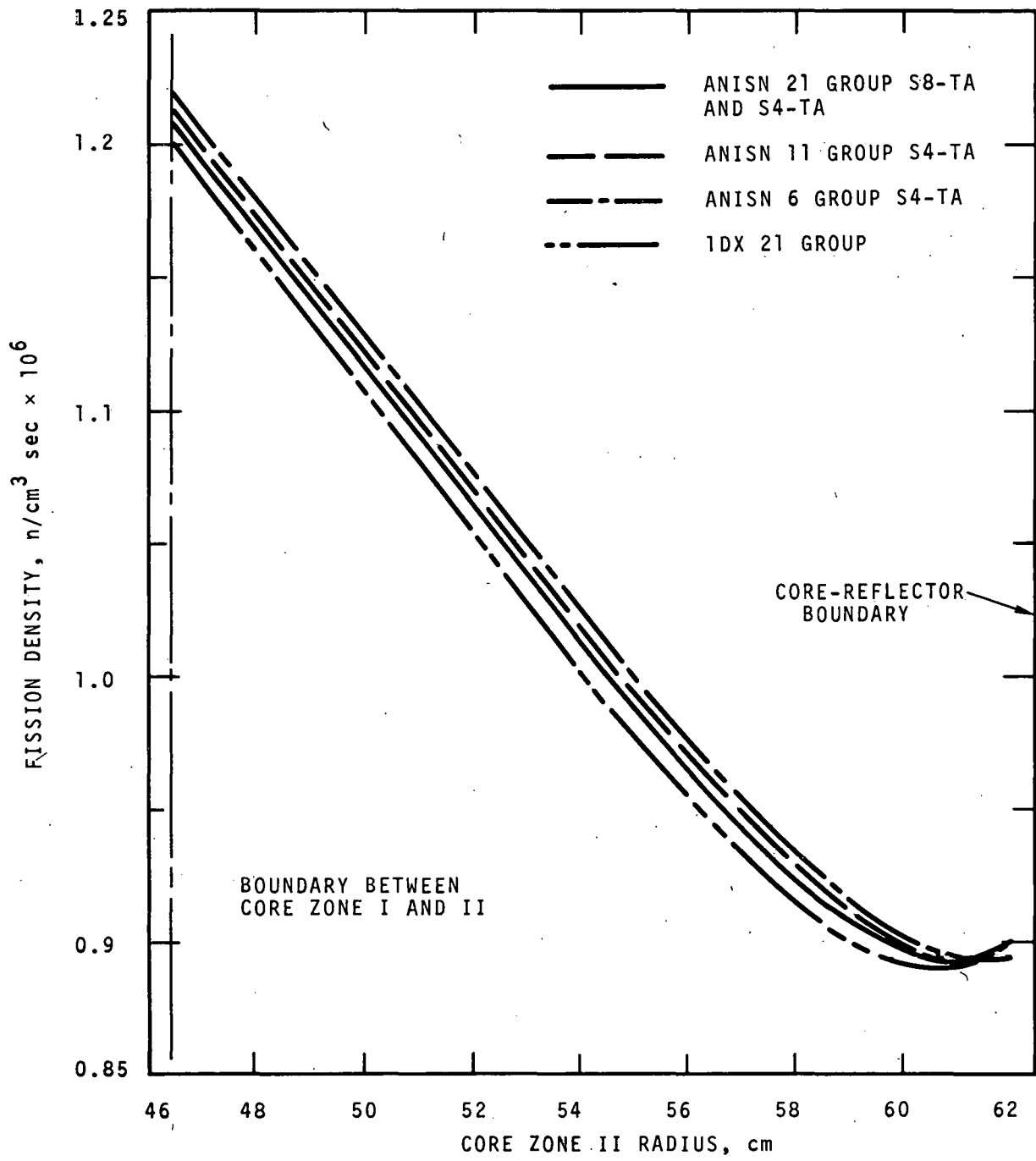


**FIGURE 2.2.** Effect of Angular Detail and Energy Resolution near Core-Reflector Interface

than half in going from 21 to 11 groups (combining the higher 20 groups by twos), and was unaffected by a further reduction to 6 groups. It appears that an accurate description of the neutron energy redistribution near the reflector requires considerably more spectral detail than is provided in the usual few-group models. It should be noted that the groups affected comprise only a small part of the total flux and, with resonance shielded cross sections, contribute only a small part of the local power density. Therefore, the effects of varying energy resolution are not readily seen in either the total flux or the local power density distribution (with shielded cross sections).

## 2.5 EFFECTS OF CROSS-SECTION RESONANCE SHIELDING

The total flux distribution decreased monotonically approaching the core-reflector interface in all calculations examined, so that any power peaking effects near the reflector were due to spectrum changes. Typical spectra at the core center and edge are shown in Figure 2.3 obtained from an S8-P3 calculation. Cross-section sets which incorporate resonance self-shielding corrections in the  $\text{Pu}^{239}$  fission cross section are naturally less sensitive to the softened spectrum near the reflector than are those for infinitely dilute materials. This difference was examined by comparing Cases 9 and 10, where an increase by a factor of 4 or 5 in the peaking effect can be attributed to the use of dilute  $\text{Pu}^{239}$  fission cross sections. This same effect is believed to account for a substantial part of the differences between power distributions calculated with the 27-group cross-section set (Cases 1 through 4) and the Russian-derived, resonance self-shielded cross sections<sup>(6)</sup> (Cases 5 through 9).

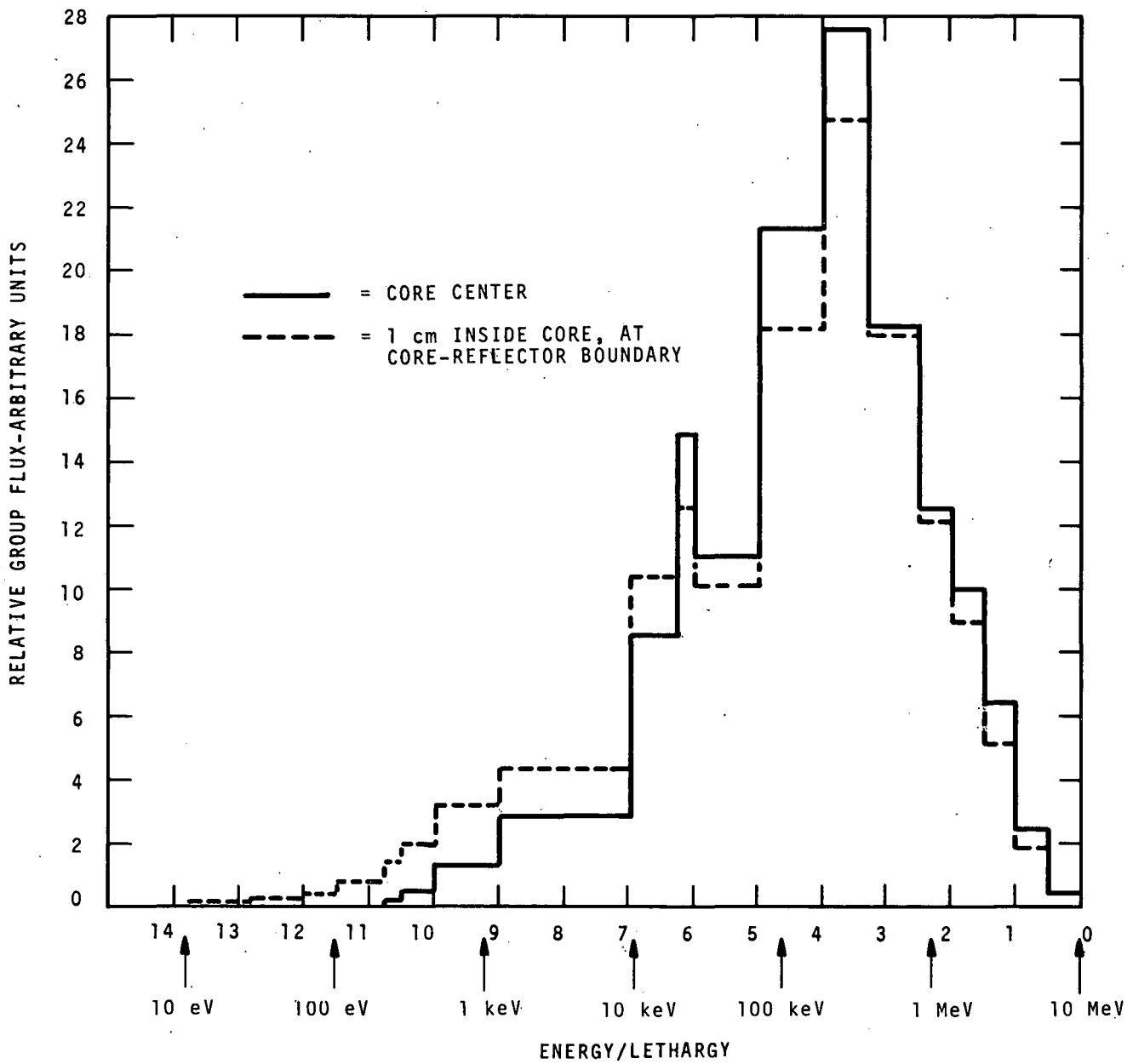


**FIGURE 2.3.** Comparison of Flux Spectra at Core Center and Core-Reflector Boundary, from Case 1 (S8-P3)

## 2.6 EFFECT OF SPATIAL RESOLUTION

The calculations listed in Table 2.1 from which the preceding conclusions were drawn were made with 1 cm mesh intervals in the vicinity of the core edge, which was sufficient to resolve the spatial distribution of group fluxes down through about 100 eV with fair accuracy. However, calculated spatial distributions for lower energy groups experienced substantial discontinuities at the core edge. Consequently, a single diffusion calculation was made using resonance shielded 26 group cross sections and 0.1 cm mesh intervals at the core edge, in which a fairly continuous spatial distribution was preserved in all groups down to about 1.0 eV. The local power density averaged over the last 0.1 cm at the core edge was calculated to be about 2 percent higher than the corresponding value averaged over a mesh interval of 1.0 cm.

## 3.0 TWO-DIMENSIONAL CALCULATIONS

### 3.1 XY CALCULATIONS

Detailed flux distributions were calculated with 2DB<sup>(3)</sup> and DOT<sup>(4)</sup> for a simple quarter core in XY geometry having two fuel enrichment zones, a reflector, and a single boron carbide peripheral poison rod (Figure 3.1). The number of mesh intervals in the control rod and each surrounding assembly was varied from 4 to 16. These calculations were all performed with the same geometry description, atom densities, and 6-group cross sections collapsed from the 26-group FTR-III set<sup>(6)</sup>. The geometry description and atom densities used were representative of a typical FTR core (see Appendix A). All calculations were normalized to a total fission neutron source rate of  $8.5 \times 10^{16}$  n/cm<sup>3</sup>-sec.

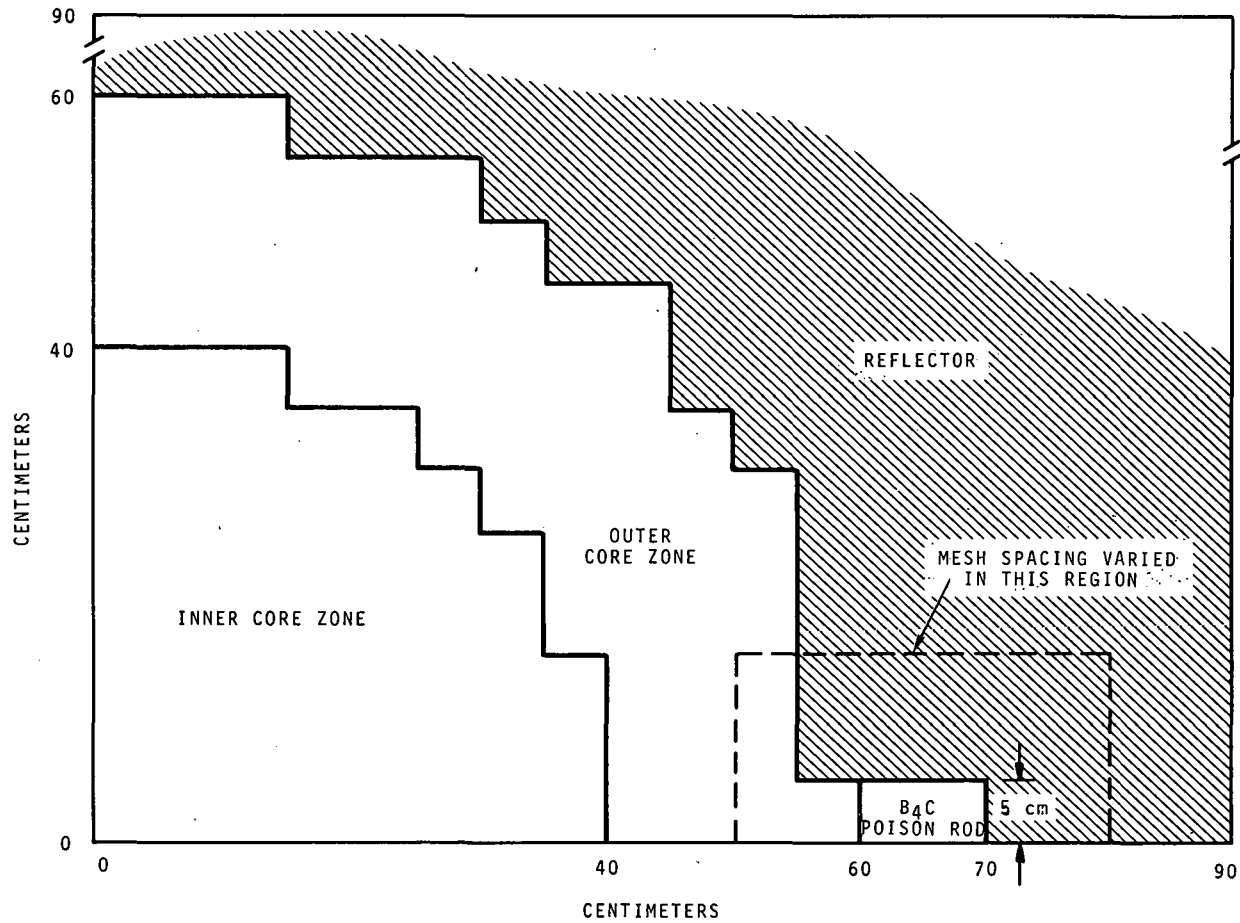


**FIGURE 3.1.** Geometry for XY Calculations

The four XY runs are tabulated in Table 3.1 along with the calculated eigenvalues and the mesh spacing used in and around the single  $B_4C$  peripheral control rod. A total flux traverse passing through the  $B_4C$  rod and one passing just outside it are shown in Figures 3.2 and 3.3 for both the  $2 \times 2$  and  $4 \times 4$  mesh spacing. A blowup of the flux traverses through the area in which the mesh spacing was varied is also shown in Figures 3.4 and 3.5. These four graphs, Figures 3.2 through 3.5, show extremely good agreement in total flux, not only between the two different codes but also between the  $2 \times 2$  and  $4 \times 4$  mesh spacing.

TABLE 3.1  
TWO-DIMENSIONAL XY CALCULATIONS

Computer Code	Calculational Approx.	Scattering Treatment	Cross Sections	Mesh Spacing	Calculated Eigenvalue
2DB	DIFF	TA <sup>(a)</sup>	6 Group	2 × 2	1.0876
2DB	DIFF	TA	6 Group	4 × 4	1.0871
DOT	S4	TA	6 Group	2 × 2	1.0877
DOT	S4	TA	6 Group	4 × 4	1.0895

a. Transport approximation cross sections

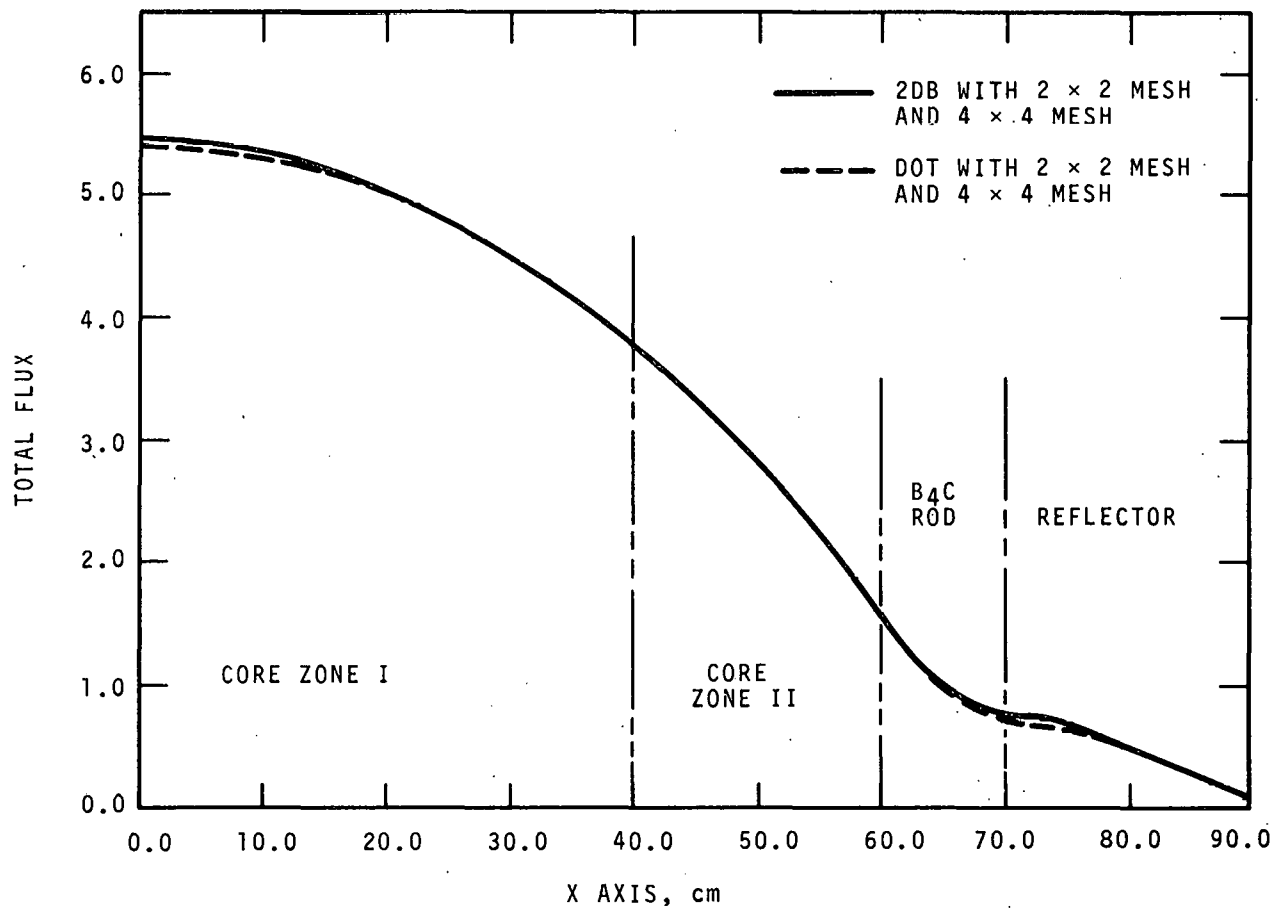


FIGURE 3.2. Total Flux Traverse Through  $B_4C$  Rod

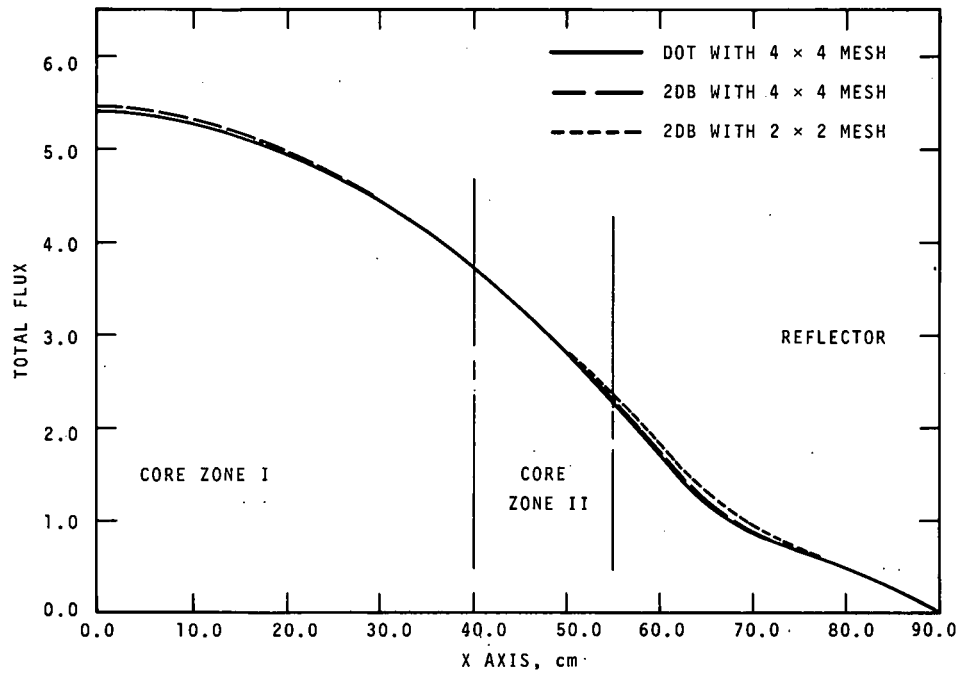


FIGURE 3.3. Total Flux Traverse Just Outside B<sub>4</sub>C Rod

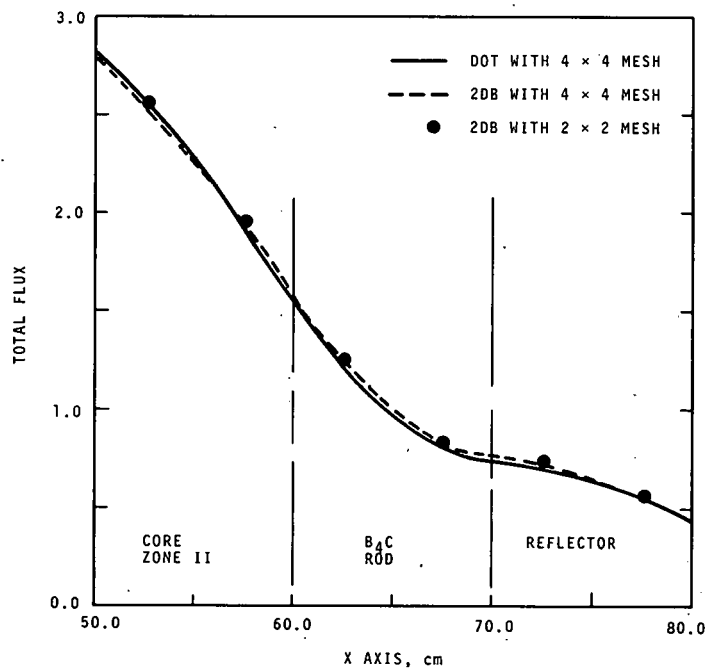


FIGURE 3.4. Blowup of Flux Traverse Through B<sub>4</sub>C Rod



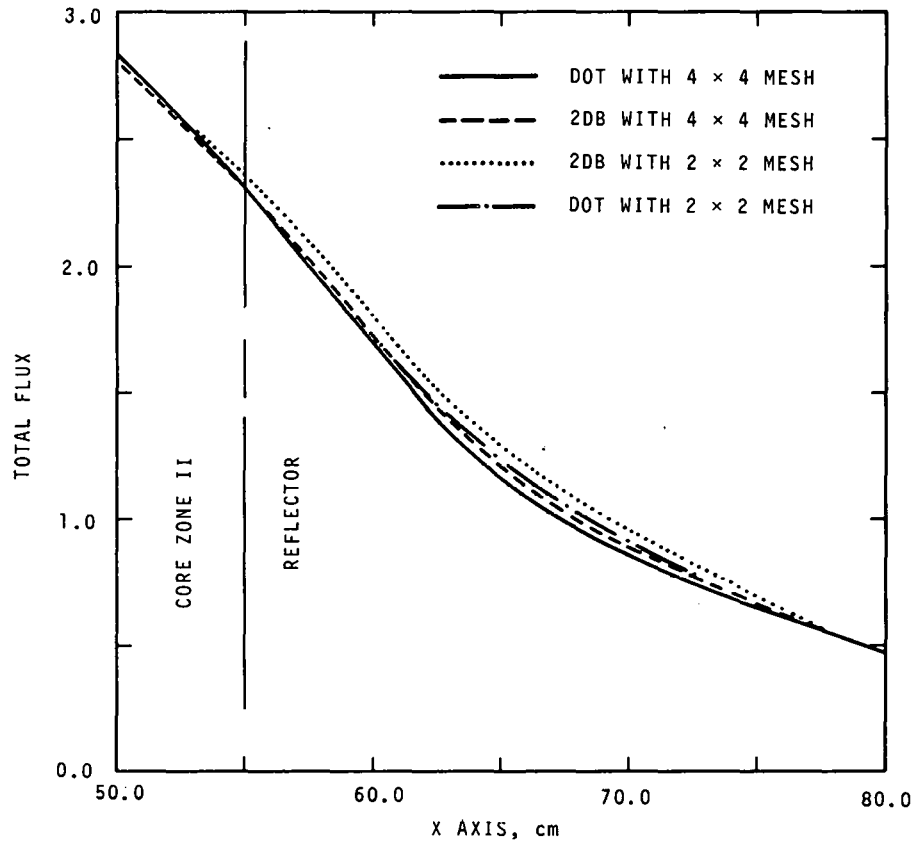
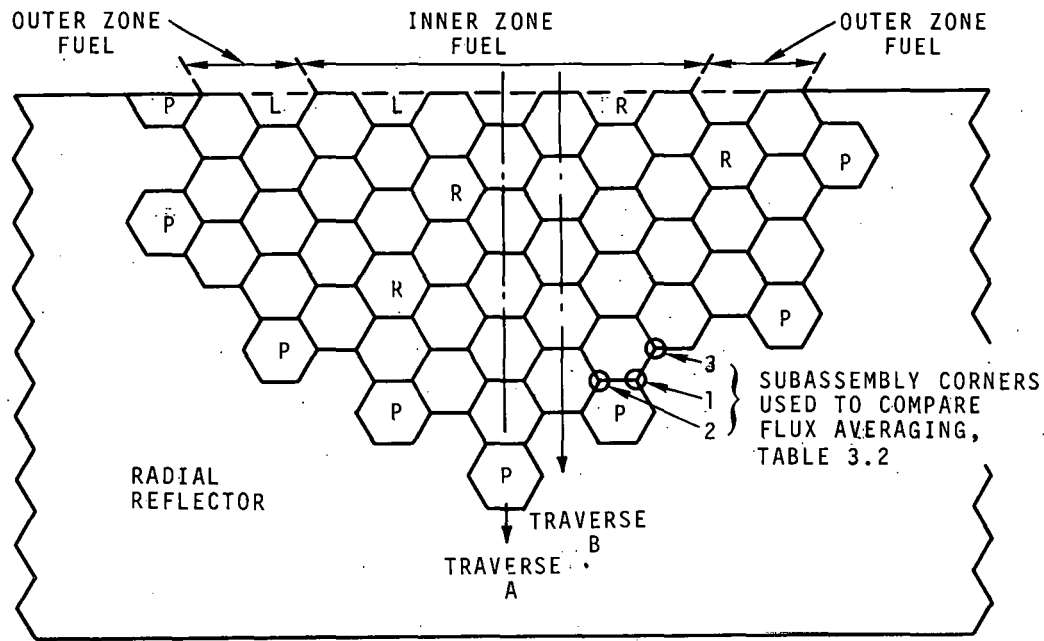


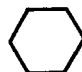
FIGURE 3.5. Blowup of Flux Traverse  
Just Outside  $B_4C$  Rod

The expected variances between diffusion and transport calculations in regions of high absorption are observed in the low energy flux distribution near the poison rod, where transport calculations yield considerably higher fluxes within and near the control rod. The energy groups affected contribute very little to the total flux, however, and both the fission density at the core edge and the total absorption rate in the poison rod were calculated accurately by diffusion theory.

### 3.2 RESULTS OF TRIANGULAR GEOMETRY CALCULATIONS

Two diffusion theory calculations in triangular geometry were made using 2DB<sup>(2)</sup>: one calculation with 6 mesh triangles per hexagonal lattice position and one with 24 mesh triangles per lattice position. The core map used is shown in Figure 3.6. Twenty-one energy groups were used, with cross sections collapsed from the 26-group FTR-III set.<sup>(6)</sup>



-  = DRIVER FUEL
- L = CLOSED LOOP
- R = IN-CORE CONTROL ROD (WITHDRAWN)
- P = PERIPHERAL  $B_4C$  POISON SECTION

CORE LATTICE = 4.715 in.

FIGURE 3.6. Half-Core Hexagonal Geometry

Total flux and power density traverses were compared from the two calculations along a line through a peripheral poison rod (A-A, in Figure 3.6) and through a reflector (B-B). The close agreement can be seen in Figures 3.7 and 3.8 where the results from the six-mesh triangle calculation are superimposed on a curve drawn through the 24-mesh results. Eigenvalues were calculated as 0.9976 with 6-mesh triangles per hexagon and 0.9947 with 24.

The influence of mesh triangle size on calculated local average flux was evaluated by comparing the average flux within a hexagonal region comprised of the six-mesh triangles immediately surrounding a fixed point (subassembly corner point) from both the 6-mesh and 24-mesh results. With the usual 6-triangle per hexagon mesh description, this averaging prescription yields the interpolated local flux at a subassembly corner as the average of the fluxes calculated for the six adjacent mesh triangles which constitute a region equivalent in size to a core lattice position. When the same procedure is applied in the 24-mesh results, the local flux at a subassembly corner is obtained by an average over a region one-fourth the size of a lattice position presumably yielding better accuracy for rapidly varying fluxes. Three subassembly corner locations were examined, identified in Figure 3.6, and interpolated (averaged) fluxes were compared for groups 8 and 15 of the Russian 26-group format (0.1 to 0.2 MeV and 0.465 to 1.0 keV, respectively).

Calculated average fluxes are shown in Table 3.2. The high energy flux is estimated with good accuracy by linear averaging over a region the size of a core lattice position, while differences up to ~20 percent occur in the low energy averaged flux due to the faster changing flux gradient near the reflector, and particularly near the peripheral poison rod. The total flux and power density distributions show little evidence of this effect due to the small contribution of low energy flux groups.

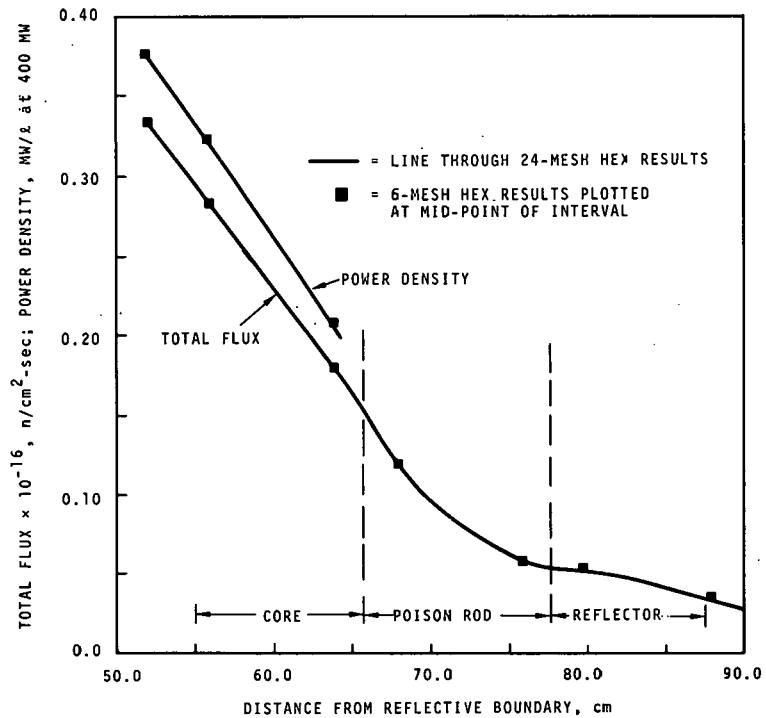


FIGURE 3.7. Total Flux and Power Density Traverse "A"

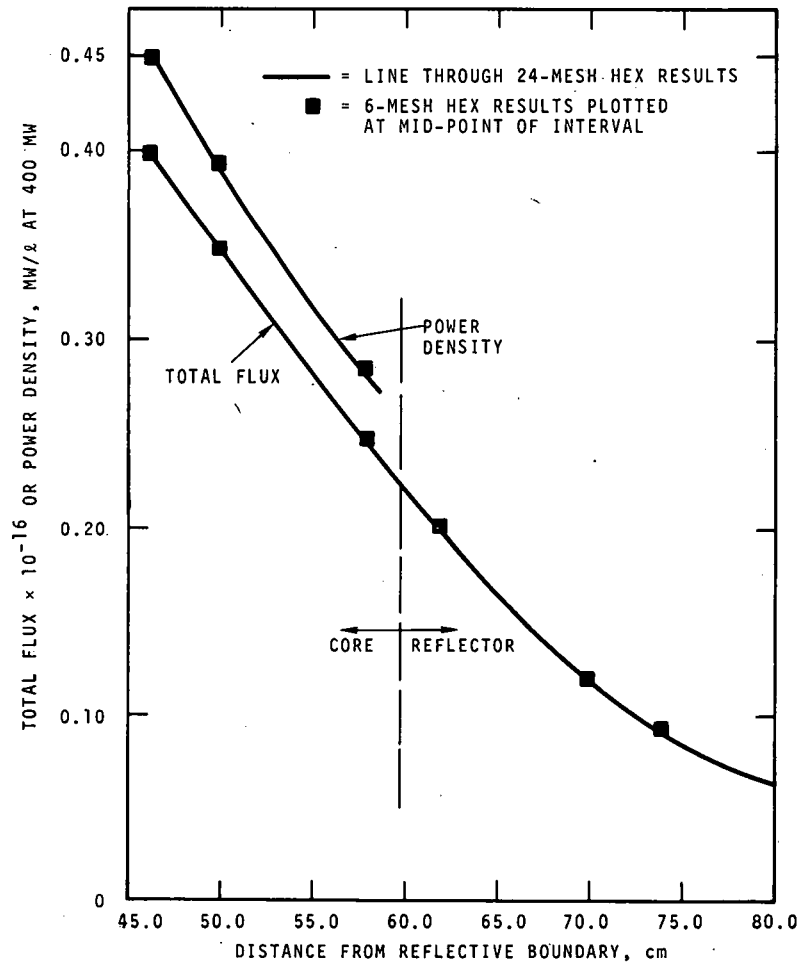


FIGURE 3.8. Total Flux and Power Density Traverse "B"

TABLE 3.2  
 AVERAGED GROUP FLUXES OBTAINED FROM 6 AND  
 24 MESH TRIANGLE PER HEXAGONAL CALCULATIONS

	Point at which Fluxes are Averaged <sup>(a)</sup>		
	Point 1	Point 2	Point 3
<u>Group 8 Averaged Flux:</u>			
6-mesh case	$0.367 \times 10^{15}$	$0.417 \times 10^{15}$	$0.471 \times 10^{15}$
24-mesh case	$0.367 \times 10^{15}$	$0.418 \times 10^{15}$	$0.473 \times 10^{15}$
% difference	0.1%	0.2%	0.5%
<u>Group 15 Averaged Flux:</u>			
6-mesh case	$0.233 \times 10^{14}$	$0.785 \times 10^{14}$	$0.347 \times 10^{14}$
24-mesh case	$0.195 \times 10^{14}$	$0.709 \times 10^{14}$	$0.329 \times 10^{14}$
% difference	19%	11%	5%

a. See Figure 3.6

#### 4.0 CONCLUSIONS

The calculations performed for this study were intended to show the effects of increased resolution in space, angle, energy, and scattering description, when compared with the few-group diffusion calculations commonly employed in FTR core nuclear analyses. In regard to the calculated flux and power distributions near the core-reflector interface, the following trends were observed:

- a) A fine space mesh ( $\sim 1$  cm) and energy resolution ( $\sim 20$  groups) were required to describe the spatially varying spectrum in sufficient detail to predict the low-energy fluxes accurately. Due to their small contribution to the total flux, the total flux distribution is

accurately calculated with relatively coarse mesh in both space and energy. Whether or not the accurate representation of the low energy flux distribution is important to the calculation of local power density near the reflector depends strongly on the low energy fission cross section. With the resonance shielded cross-section set, the influence of the spatial distribution of low energy flux is weak and the local power density is judged to be well represented in a four to six group calculation in triangular geometry with six-mesh triangles per hexagon.

- b) Given adequate space and energy resolution, the comparison of cases calculated with varying degrees of angular resolution in flux and scattering anisotropy shows the low order calculations (S2 or diffusion theory) consistently exaggerate any tendency toward local power peaking due to spectrum softening near the reflector. This exaggeration appears to result from both a higher total flux near the core-reflector interface and a slightly softer spectrum, when calculated by lower order theory. While diffusion calculations do not predict the flux distributions correctly near strong absorbers, this consideration affects only the low energy groups which do not contribute significantly to the total flux, fission rate, or poison rod absorption rate.
- c) Local group fluxes at subassembly corners in triangular geometry can be interpolated accurately in the higher energy groups by averaging the flux values in the surrounding six mesh triangles with a mesh of six triangles per hexagonal lattice position. A smaller interpolation interval is required for low energy group fluxes ( $\sim 1$  keV) near the reflector. Local power density is accurately calculated with a mesh of six triangles per hexagonal lattice position, despite inaccuracies in the low energy group fluxes near the reflector.

REFERENCES

1. R. W. Hardie and W. W. Little, Jr. 1DX, A One-Dimensional Diffusion Code for Generating Effective Nuclear Cross Sections, BNWL-954, Battelle-Northwest, Richland, Washington, 1969.
2. W. W. Little, Jr., and R. W. Hardie. 2DB User's Manual -- Revision 1, BNWL-831 Rev. 1. Battelle-Northwest, Richland, Washington, 1969.
3. W. W. Engle. A User's Manual for ANISN, A One-Dimensional Discrete Ordinates Transport Code with Anisotropic Scattering, K-1693. Oak Ridge National Laboratory, Oak Ridge, Tennessee, 1967.
4. F. P. Mynatt. A User's Manual for DOT, A Two-Dimensional Discrete Ordinates Transport Code with Anisotropic Scattering, K-1694. Union Carbide Corporation, Oak Ridge, Tennessee, October, 1969.
5. C. E. Lee. The Discrete Sn Approximation to Transport Theory, LA-2595, Los Alamos Scientific Laboratory, Los Alamos, New Mexico, 1962.
6. J. V. Nelson and S. L. DeMyer. Group Constants for Analysis of FFTF Critical Experiments, BNWL-1044. Battelle-Northwest, Richland, Washington, 1969; I. I. Bondarenko, ed. Group Constants for Nuclear Reactor Calculations, Consultants Bureau, New York, 1964.
7. R. W. Hardie and W. W. Little, Jr. PERT-V, A Two-Dimensional Perturbation Code for Fast Reactor Analysis, BNWL-1162. Battelle-Northwest, Richland, Washington, September, 1969.
8. K. D. Lathrop. "Anisotropic Scattering Approximations in the Monoenergetic Boltzmann Equation", Nuclear Science and Engineering, vol. 21, p. 498, 1965.



## APPENDIX A

CALCULATIONAL MODEL DETAILS1. ONE-DIMENSIONAL CORE MODELGeometry: Spherical, Two core enrichment zones plus reflector

Inner enrichment zone radius: 43.35 cm

Outer enrichment zone radius: 61.45 cm

Reflector outer radius: 99.18 cm

Mesh intervals: 3.1 cm - interior

1.0 cm - near core-reflector  
boundary2. COMPOSITIONS: (Atom densities per barn-cm)

<u>Material</u>	<u>Inner Core Zone</u>	<u>Outer Core Zone</u>	<u>Reflector</u>
Pu <sup>239</sup>	0.001277	0.001535	0.0
Pu <sup>240</sup>	0.000174	0.0002093	0.0
U <sup>235</sup>	0.00004	0.0000378	0.0
U <sup>238</sup>	0.005671	0.00536	0.0
O	0.01443	0.01447	0.0
Cr	0.00363	0.00363	0.01312
Fe	0.01422	0.01422	0.01556
Ni	0.00227	0.00227	0.04606
Na	0.009098	0.009098	0.00336

<u>Material</u>	<u>B<sub>4</sub>C Rod</u>	<u>Rod Follower</u>
B <sup>10</sup>	0.007424	0.0
B <sup>11</sup>	0.02970	0.0
C	0.009281	0.0
Cr	0.004330	0.01011
Fe	0.01697	0.01942
Ni	0.002710	0.02764
Na	0.007276	0.007276

DISTRIBUTIONNo. of  
Copies  
OFFSITE

1 AEC Chicago Patent Group  
G. H. Lee, Chief

28 AEC Division of Reactor Development and Technology  
Director, RDT  
Asst Dir for Nuclear Safety  
Analysis & Evaluation Br, RDT:NS  
Asst Dir for Plant Engrg, RDT  
Facilities Br, RDT:PE  
Components Br, RDT:PE  
Instrumentation & Control Br, RDT:PE  
Liquid Metal Systems Br, RDT:PE  
Asst Dir for Program Analysis, RDT  
Asst Dir for Project Mgmt, RDT  
Liquid Metals Projects Br, RDT:PM  
G. J. Mishko  
FFTF Project Manager, RDT:RE  
Asst Dir for Reactor Engrg, RDT  
Control Mechanisms Br, RDT:RE  
Core Design Br, RDT:RE (2)  
T. E. Murley  
Fuel Engineering Br, RDT:RE  
Fuel Handling Br, RDT:RE  
Reactor Vessels Br, RDT:RE  
Coolant Chemistry Br, RDT:RT  
Fuel Recycle Br, RDT:RT  
Fuels & Materials Br, RDT:RT  
Reactor Physics Br, RDT:RE  
Special Technology Br, RDT:RT  
Asst Dir for Engrg Standards, RDT  
LMFBR Program Manager, RDT:PM

1 AEC Idaho Operations Office  
Nuclear Technology Division  
C. W. Bills, Director

1 AEC San Francisco Operations Office  
Director, Reactor Division

5 AEC Site Representatives  
Argonne National Laboratory - CH  
Argonne National Laboratory - ID  
Atomics International  
General Electric Company  
Westinghouse Electric Corp

No. of  
Copies

215 AEC Division of Technical Information Extension

3 Argonne National Laboratory  
R. A. Jaross  
LMFBR Program Office  
N. J. Swanson

1 Argonne National Laboratory (Idaho)  
R. M. Fleishman (WADCO Rep)

1 Atomic Power Development Association  
Document Librarian

1 Atomics International  
FFTF Program Office

2 Babcock & Wilcox Company  
Atomic Energy Division  
S. H. Esleeck  
G. B. Garton

5 Bechtel Corporation  
J. J. Teachnor

1 Combustion Engineering  
1000 MWe Follow-On Study  
W. P. Staker, Project Manager

1 Combustion Engineering  
Mrs. Nell Holder, Librarian

4 General Electric Company  
Advanced Products Operation  
Karl Cohen (3)

1 General Electric Company  
Nucleonics Laboratory  
Dr. H. W. Alter, Mgr.

2 Gulf General Atomic Inc.  
General Atomic Division  
D. Coburn

1 Idaho Nuclear Corporation  
J. A. Buckham

1 Liquid Metal Engineering Center  
R. W. Dickinson

2 Liquid Metal Information Center  
A. E. Miller

No. of  
Copies

2     Oak Ridge National Laboratory  
       W. O. Harms

1     Stanford University  
       Nuclear Division  
       Division of Mechanical Engrg  
       R. Sher

1     United Nuclear Corporation  
       Research and Engineering Center  
       R. F. DeAngelis

11    Westinghouse Electric Corporation  
       Atomic Power Division  
       Advanced Reactor Systems  
       D. C. Spencer (10)  
       L. E. Strawbridge

ONSITE

1     AEC Richland Operations Office  
       J. M. Shivley

1     AEC Chicago Patent Group  
       R. K. Sharp (Richland)

7     Battelle-Northwest  
       BNW Technical Information Files (5)  
       BNW Technical Publications (2)

2     RDT Asst Dir for Pacific Northwest Programs  
       T. A. Nemzek

52    WADCO Corp.  
       R. A. Bennett  
       W. L. Bunch  
       W. M. Gajewski  
       R. W. Hardie  
       R. E. Heineman  
       R. J. Hennig  
       P. L. Hofmann  
       D. C. Kolesar  
       F. J. Leitz  
       W. W. Little, Jr.  
       L. D. O'Dell (20)  
       R. P. Omberg  
       R. B. Rothrock  
       A. E. Waltar  
       J. E. Werle  
       J. F. Wett  
       B. Wolfe  
       WADCO Document Control (15)  
       WADCO Tech Pubs (703 Bldg.)